ACS OMEGA

http://pubs.acs.org/journal/acsodf

Article

Efficient Synthesis of α-FeOOH from Pickling Wastewater in Falling Film Tower and Its Kinetics

Jian Chen, Fuwei Xiang, Mengjing Zhu, Junfeng Li, Hongjun Yang, Yuanyuan Che,* and Zhipeng Mao*

Cite This: *ACS Omega* 2021, 6, 8394−8402

Read Online

ACCESS | Metrics & More | Article Recommendations | Supporting Information

ABSTRACT: An efficient way to synthesize α-FeOOH from pickling wastewater in a falling film tower was proposed for the first time. This method overcomes the shortcomings of the traditional air oxidation method, and its production efficiency is increased by 16 times. The purity of α-FeOOH synthesized from pickling wastewater can reach 96.3%, and the iron recovery rate is greater than 90%. At the same time, we have systematically studied its kinetics in the falling film tower. The reaction rate constant k at different temperatures was also determined with the activation energy E_a = 32.2497 kJ/mol and the pre-exponential A = 47.4132 s^{-1}. In addition, based on the double-film theory, a corresponding macrokinetic model was established. Also, the Hatta number in the reaction system was obtained, which proved the excellent gas−liquid mass transfer performance in the falling film tower. This work provides a promising method for the efficient production of α-FeOOH and the recycling of pickling wastewater.

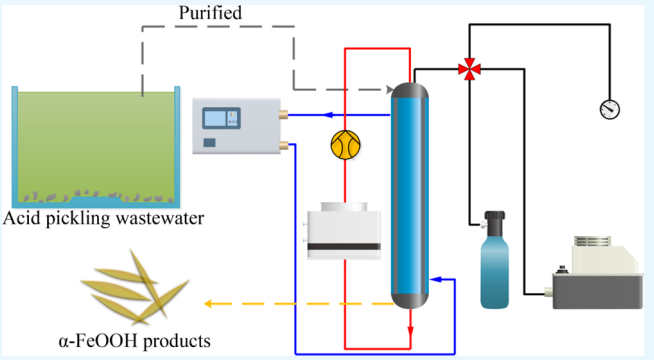

1. INTRODUCTION

α-FeOOH nanoparticles have attracted much attention due to their special properties, such as optical properties, corrosion resistance, and biocompatibility.[1−4] It is suitable for the field of anticorrosion, adsorption, catalysis, and biomedicine.[5−8] Meanwhile, α-FeOOH is also an important intermediate product to synthesize α-Fe_2O_3, Fe_3O_4, and magnetic materials.[9,10] Amani-Ghadim et al.[11] synthesized α-FeOOH nanoparticles for photocatalytic decomposition of azo dyes, and Zhang et al.[12] combined air oxidation with bipolar membrane electrodialysis to prepare α-FeOOH with a highly improved oxidation efficiency. The batch air oxidation method is commonly used in the industry to synthesize α-FeOOH, which usually requires continuous ventilation for more than 24 h.[12,13] This method suffers from the shortcomings of high energy consumption, long reaction period, and low yield. The reaction equation for the synthesis of α-FeOOH is shown in eq 1, which is a multiphase reaction. The mass transfer process is very complicated and plays an important role in the reaction.

$$4Fe^{2+}(aq) + 6H_2O(l) + O_2(g) \rightarrow 4FeOOH(s) + 8H^+(aq) \quad (1)$$

Therefore, we proposed a falling film tower to improve the gas−liquid mass transfer efficiency, and a pure oxygen atmosphere was used to promote the oxidation reaction efficiency. The falling film tower is a commonly used gas−liquid reaction device. The liquid phase flows slowly down the surface of the tower wall in the form of a thin liquid film under the action of gravity and makes contact with the gas phase to react. The schematic diagram of the falling film tower device is shown in Figure 1. The device includes a falling film tower as the main reaction zone. A liquid distributor is installed on the top of the falling film tower to ensure uniform distribution of liquid along the wall of the tower. There is no extra structure in the middle of the falling film tower, which can ensure the even distribution of gas. The inner diameter of the falling film tower is 12 mm, the height is 1000 mm, and it has an insulation jacket to ensure the stable reaction temperature of the tower wall. The peristaltic pump can transport the reaction liquid to the top of the tower, and an oxygen cylinder provides a source of oxygen. The gas valve can control each gas path, and the lye storage tank is used to control the pH of the reaction solution. The red line in the figure is the circulation path of the reaction solution, and the blue line is the circulation path of insulated water. The falling film tower has attracted extensive attention due to its characteristics of small temperature difference and high mass transfer efficiency.[14,15] In addition, there are no moving parts inside; the structure is simple and not easy to block,[16] thus avoiding the shortcomings of the packed tower,

Received: January 8, 2021
Accepted: March 5, 2021
Published: March 16, 2021

https://dx.doi.org/10.1021/acsomega.1c00125
ACS Omega 2021, 6, 8394−8402

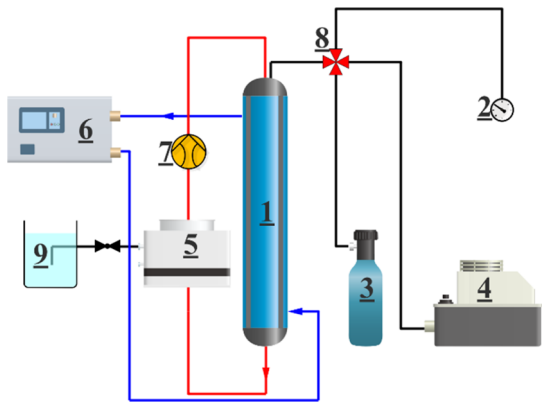

Figure 1. Diagram of falling film tower reaction device: (1) falling film tower; (2) differential pressure gauge; (3) oxygen cylinder; (4) vacuum pump; (5) preheating device; (6) thermostatic sink; (7) peristaltic pump; (8) three-way valve; (9) lye tank.

such as large gas−liquid resistance and gas−liquid interception.[17,18] At present, there are few studies on the synthesis kinetics of α-FeOOH and even less on the macrokinetics considering the influence of mass transfer. Domingo et al.[19] studied the oxidation kinetics of different iron oxides. Legg et al.[20] studied the microscopic nucleation process of iron oxyhydroxide nanoparticles. Therefore, it is very essential to carry out research on the kinetics of the synthesis of α-FeOOH.[21,22] How to improve the mass transfer efficiency is the key point to improve production efficiency.[23,24] In this study, the macrokinetics in the falling film tower system was investigated to better understand the effect of high mass transfer efficiency on the reaction rate.

The pickling wastewater is produced during the pickling process of steel; it has strong acidity and contains around 60−250 g/L of Fe^{2+}.[25,26] The Fe^{2+} of pickling wastewater is generated by the reaction of acid and steel during the pickling process, and the pH range of the pickling wastewater is around 1−2. It will cause severe environmental pollution and waste of resources if not treated appropriately. Millions of tons of pickling wastewater are generated every year, and the most commonly used method for industrial treatment of pickling wastewater is the neutralization method, which will cause huge consumption and secondary pollutants.[27,28] More attention has been paid to the recovery and utilization of acid pickling wastewater, such as recovery of HCl by membrane distillation.[29,30] In order to recycle wastewater and obtain valuable products, we have newly developed a method to synthesize α-FeOOH from pickling wastewater in the falling film tower. In this way, the resourceful and harmless treatment of the acid pickling wastewater was fully realized with higher efficiency and lower cost. This research is of great significance for the reasonable recycling of pickling wastewater and improving the production efficiency of α-FeOOH.

2. RESULTS AND DISCUSSION

2.1. Experimental Results and Characterization. First, we studied the conditions for the synthesis of α-FeOOH by batch air oxidation to ensure that the conditions are applicable to the falling film tower system. The batch air oxidation mainly uses ferrous salt solution as the raw material, and the oxidation reaction is carried out by blowing air into a kettle reactor (the air oxidation reaction device can be seen in the Supporting Information). During the reaction process, the pH value of the reaction solution needs to be adjusted within a certain range to ensure the purity of the product. We optimized the batch air oxidation and got the best conditions as temperature 80 °C, stirring speed 400 rpm, and air flow rate 2 L/min. Then, under these conditions, the effect of pH on the reaction was explored. The purified pickling water was mixed with distilled water to adjust its ferrous concentration to 0.5 mol/L. The pH of the purified pickling water is around 2−3; alkali was added to adjust the initial pH to 5. During the reaction process, no alkali was added to observe the pH value of the solution changes over time. It can be seen from Figure 2 that the pH of solution

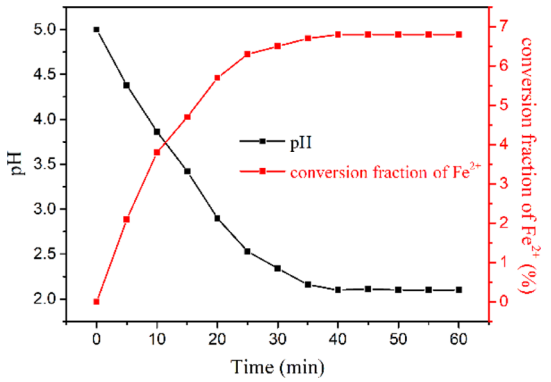

Figure 2. Change of the pH value with time without adding alkali.

continues to decrease as the reaction proceeds and finally stabilizes at around 2.1. Figure 2 also describes the change of the conversion fraction of ferrous iron with time, indicating that the reaction rate slows down as the pH value decreases and finally stops gradually. This is because H^+ is generated during the reaction. The ferrous iron content in the solution is titrated by $K_2Cr_2O_7$.

Figure 3 shows the XRD patterns of synthesized products in different pH ranges. Figure 3a is the XRD pattern of products synthesized with a pH value controlled between 4 and 5, which is consistent with the standard PDF card of α-FeOOH. It can be concluded from Figure 3b-B that amorphous miscellaneous crystals without obvious characteristic peaks are easily formed between pH 5−6, such as ferrihydrite. In the pH range of 6−8, it can be seen from Figure 3b-A that mixed crystals dominated by maghemite are formed. The pH value has a significant impact on the synthesis of α-FeOOH; the reaction rate is faster under higher pH conditions, and the products are very different in different pH ranges. Therefore, it is necessary to maintain the pH within a stable range; the following experiments are controlled in an optimal pH range of 4−5.

We explored the reaction efficiency of three different reaction systems, namely, batch air oxidation, tower counter flow, and tower oxygen atmosphere. The batch air oxidation method is the same as much as the industrial one, using the agitated aeration reaction in the kettle. Tower counter flow and tower oxygen atmosphere are both carried out in the same falling film tower. The tower counter flow uses an air pump to blow air from the bottom of the tower, and the liquid phase flows down from the top of the tower as a falling film; the gas−liquid phase react by countercurrent contact. The tower oxygen atmosphere adopts a pure oxygen atmosphere in a closed system; the gas phase is static and the liquid phase flows down from the top of the tower as a falling film, that is, the tower oxygen atmosphere has a higher oxygen concentration.

https://dx.doi.org/10.1021/acsomega.1c00125
ACS Omega 2021, 6, 8394−8402

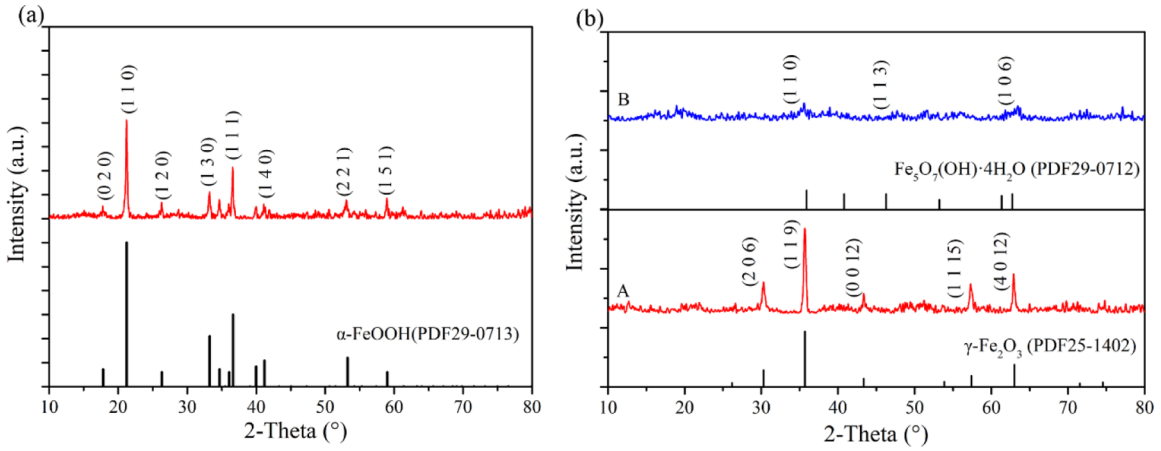

Figure 3. XRD patterns of products generated in different pH ranges: (a) pH range 4−5; (b-A) pH range 6−8 and (b-B) pH range 5−6.

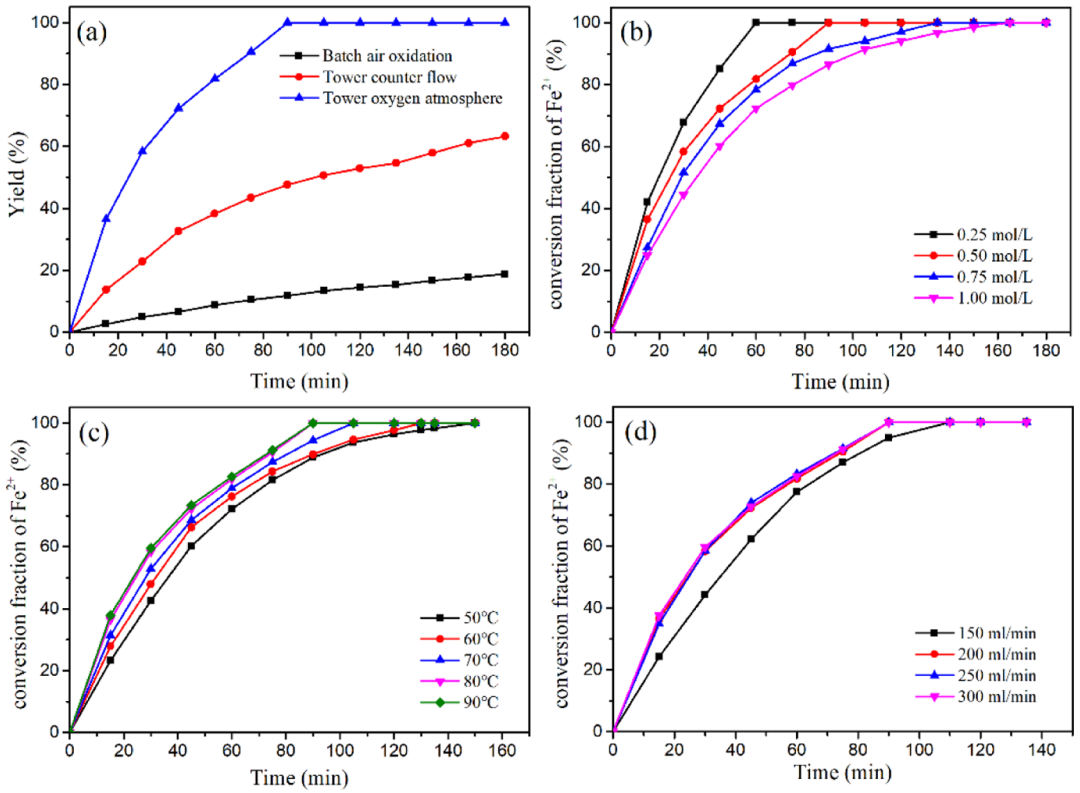

Figure 4. Effect of reaction conditions on the reaction rate: (a) comparison of reaction rates in different reaction systems; (b) initial concentration of the reaction solution; (c) temperature; (d) liquid flow rate.

The difference between the two is the gas−liquid contact mode and the concentration of oxygen. Figure 4a reflects the reaction efficiency of three different reaction systems. The batch air oxidation only reacted 18.8% in 3 h, while the tower counter flow can reach a yield of 63.2%, and the tower oxygen atmosphere only needs 1.5 h to complete the reaction. Based on the advantages of the falling film tower, the tower oxygen atmosphere increases the reaction efficiency several times, which greatly eliminates the shortcomings of the air oxidation method. This is because the traditional air oxidation method has a very limited gas−liquid contact area and the inhomogeneity of heterogeneous reaction. In particular, the formation of solid products further reduces the effect of stirring, and the aggregation of solid products hinders gas−liquid contact. All these have led to its low gas−liquid mass transfer efficiency and reaction rate. Due to the amplification effect in the industry, industrial production usually takes 40−50 h to complete a batch of the reaction. Compared to batch air oxidation, the falling film tower has a larger gas−liquid contact area, and the reaction liquid has the same probability of contact with the gas phase in the falling film tower. Especially, in the pure oxygen atmosphere, the mass transfer resistance is greatly reduced, so the reaction efficiency in the falling film tower is greatly improved. Based on the above experimental phenomena, we believe that the oxidation of Fe(II) to Fe(III) is the rate-limiting step because increasing the oxygen concentration can lead to a significant increase in the reaction rate. If the conversion of Fe(III) (aq) to FeOOH

https://dx.doi.org/10.1021/acsomega.1c00125
ACS Omega 2021, 6, 8394−8402

(s) is the rate-limiting step, the effect of increasing temperature on increasing the reaction rate should be significantly greater than increasing the oxygen concentration.

Then, we studied the influence of temperature, concentration, and flow rate on the reaction under tower oxygen atmosphere. Figure 4d shows the effect of the liquid flow rate on the reaction rate. The results show that when the liquid flow rate exceeds 200 mL/min, the liquid flow rate is no longer a factor limiting the reaction rate, and its influence can be ignored. In the subsequent reactions, the liquid flow rate used was 200 mL/min. It can be clearly seen from Figure 4c that the higher the temperature, the faster the reaction rate. However, when the temperature exceeds 80 °C, the reaction rate does not increase significantly. In order to reduce energy consumption, the optimal reaction temperature is 80 °C. Figure 4b indicates the time required to complete the reaction at different concentration gradients. Under the optimal temperature and liquid flow rate, the reaction with an initial concentration of 1 mol/L can be completed in only 3 h, and the concentration of 0.25 mol/L only needs 60 min.

After repeated experiments to optimize the reaction conditions, the production efficiency of the tower oxygen atmosphere is at least 4 times higher than that of tower counter flow and at least 16 times that of the traditional batch air oxidation method. This method provides an efficient way for the production of α-FeOOH. The energy consumption and cost of the oxygen atmosphere are greatly reduced compared with the air oxidation method, which is more economical and environmentally friendly. The production efficiency of the three reaction systems are listed in Table 1.

Table 1. Comparison of α-FeOOH Production Efficiency in Different Reaction Systems

reaction systems	concentration (mol/L)	reaction time (h)	yield (%)
batch air oxidation	0.5	24	85.2
tower counter flow	0.5	6	99.9
tower oxygen atmosphere	1.0	3	99.9

The crystal structures of α-FeOOH were characterized by XRD. The XRD patterns are provided in Figure 5. All the characteristic peaks at around 17.796, 21.223, 26.322, 33.241, 36.649, 41.186, 53.237, and 59.023° matched well with the

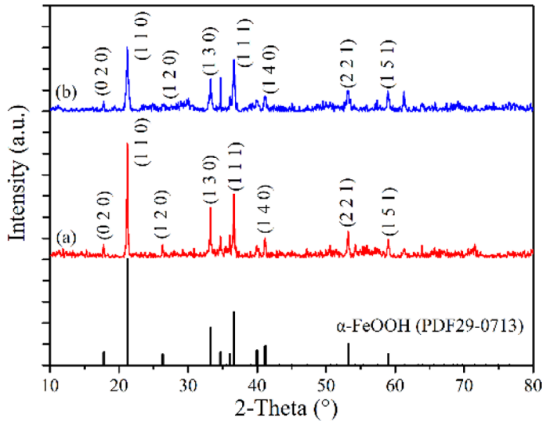

Figure 5. XRD patterns of α-FeOOH: (a) synthesized from ferrous sulfate; (b) synthesized from purified pickling wastewater.

(020), (110), (120), (130), (111), (140), (221), and (151) diffraction crystal planes of standard α-FeOOH (PDF 29-0713), respectively, indicating the high purity and crystallinity of α-FeOOH.

In Figure 5a is the XRD pattern of α-FeOOH synthesized from ferrous sulfate, and Figure 5b is the XRD pattern of α-FeOOH synthesized from purified pickling wastewater. Both of them were synthesized under optimal conditions in the falling film tower. By comparing the XRD patterns of α-FeOOH synthesized from ferrous sulfate and purified pickling wastewater, the position and intensity ratio of the characteristic peaks of the two are basically the same, which is consistent with the standard PDF card of α-FeOOH. The content of α-FeOOH was detected by atomic absorption spectroscopy (AAS), and the purity of α-FeOOH obtained from purified pickling wastewater can reach 96.3%. The results show that the purified pickling wastewater has no effect on the reaction products, and the iron recovery rate in the whole process is greater than 90%, so this process can be used as an effective method for the synthesis of α-FeOOH from the pickling wastewater.

Figure 6 illustrates typical transmission electron microscopy (TEM) images of the α-FeOOH crystals. The α-FeOOH

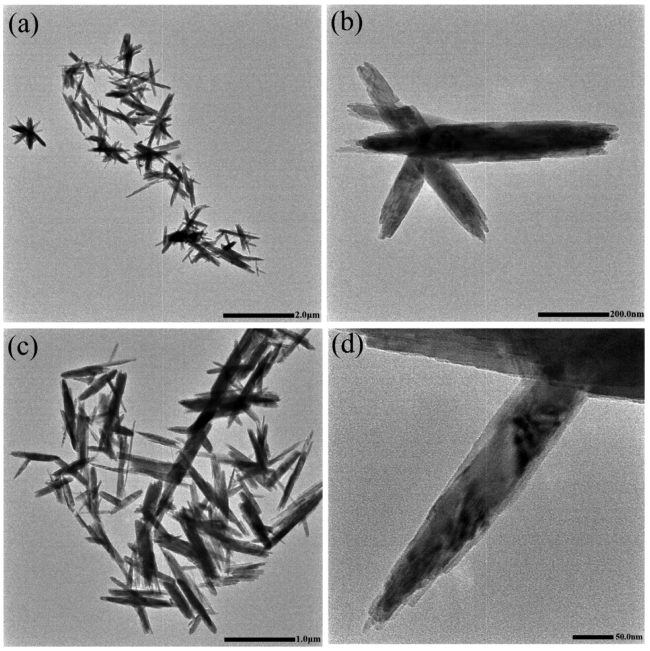

Figure 6. TEM images of α-FeOOH crystals: (a,b) α-FeOOH crystals synthesized from ferrous sulfate; (c,d) α-FeOOH crystals synthesized from purified pickling wastewater.

crystals synthesized from purified pickling wastewater are not much different from the α-FeOOH crystals synthesized from ferrous sulfate, both of which show acicular particles. Figure 6a–c shows that the acicular crystals tend to clump together to form agglomerates. An acicular crystal with good morphology can be seen in Figure 6b–d. According to statistics, the particle diameter distribution is 40–120 nm, the length ranges from 400 to 1000 nm, and the aspect ratio varies from 7:1 to 11:1. The diameter distribution of α-FeOOH crystals is shown in Figure 7.

2.2. Intrinsic Kinetics. The kinetic experimental part used pure $FeSO_4$ solution to ensure the accuracy of the kinetic data.

https://dx.doi.org/10.1021/acsomega.1c00125
ACS Omega 2021, 6, 8394–8402

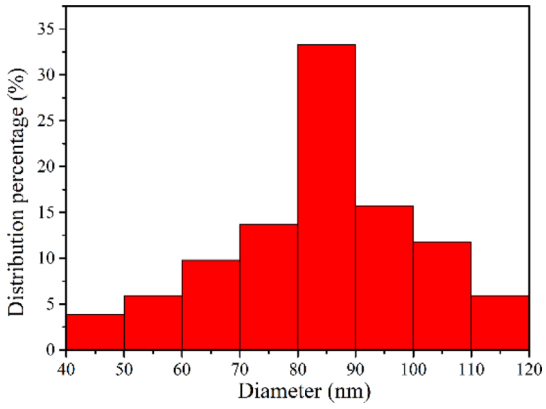

Figure 7. Diameter distribution of α-FeOOH crystals.

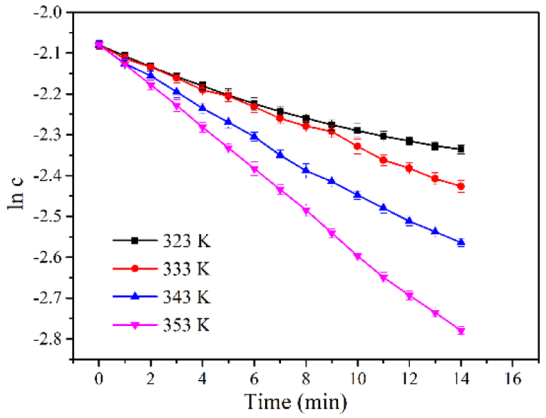

Figure 8. ln $c-t$ relationship diagram at various temperatures.

Because the reaction rate is greatly affected by the pH value, the reaction pH value is controlled at around 4.6. The kinetic reaction temperature was 323−353 K, the system pressure was 1 atm, the solution concentration was 0.1 mol/L, and the liquid flow rate was 12 L/h. The precision differential pressure gauge was connected to detect the reaction rate at different temperatures through the change of oxygen pressure. The initial pressure of oxygen in the reaction system was 101.67 kPa, and the pressure at the end of the reaction was only decreased by 1.58 kPa, which accounted for less than 2% of the total pressure. The change in oxygen pressure is negligible to the total oxygen pressure, and the total oxygen pressure can be regarded as the standard atmospheric pressure. The reaction equation is as follows

$$4Fe^{2+}(aq) + 6H_2O(l) + O_2(g) \rightarrow 4FeOOH(s) + 8H^+(aq) \quad (2)$$

The kinetic model can be expressed as eq 3

$$r = kp_{O_2}^{\alpha} c_{Fe^{2+}}^{\beta} \quad (3)$$

Constant volume, constant temperature, and closed reaction system are adopted in this experiment. The reaction system is a pure oxygen atmosphere, the oxygen in the gas phase is greatly excessive, and the change of oxygen pressure during the reaction is negligible. Therefore, it is assumed that the reaction is zero order for oxygen pressure. Domingo et al. have studied the oxidation reaction of iron oxide as a first-order reaction.[19] Accordingly, assuming that Fe(II) has pseudo-first-order kinetic characteristics, the reaction rate expression is simplified as follows

$$-\frac{dc}{dt} = kc_{Fe^{2+}} \quad (4)$$

$$-\frac{1}{c}dc = k\,dt \quad (5)$$

Take the logarithm of the eq 5 to get eq 6

$$\ln c = -kt + C \quad (6)$$

During the reaction, oxygen and Fe^{2+} are consumed in a certain stoichiometric ratio. In a closed system, according to the law of conservation of mass and the equation of state of ideal gas, the change in the oxygen content and Fe^{2+} concentration can be obtained. The experiment proved that this method has good correlation. It can be seen from Figure 8 that ln $c-t$ showed a good linear relationship at different temperatures, and the fitting degree increases with the increase of temperature. The linear fitting degree R^2 at 353 K can reach more than 0.999, which can prove that the reaction is a pseudo-first-order kinetic characteristic of Fe^{2+} concentration, and the assumptions made earlier are valid. The reaction rate constant k at different temperatures can be obtained from the slope of the straight line in Figure 8. The results are listed in Table 2. The unit of t in the kinetic equations is min^{-1}.

Table 2. Kinetic Equations and Reaction Rate Constant k at Different Temperatures

temperature (K)	kinetic equations	reaction rate constant k (s^{-1})
323	$\ln c = -0.0178t - 2.0794$	2.9617×10^{-4}
333	$\ln c = -0.0239t - 2.0794$	3.9833×10^{-4}
343	$\ln c = -0.0348t - 2.0794$	5.8000×10^{-4}
353	$\ln c = -0.0488t - 2.0794$	8.1333×10^{-4}

The activation energy E_a and pre-exponential factor A of the reaction can be calculated according to the Arrhenius equation, as shown in eqs 7 and 8. By plotting ln k and $1/T$ at different temperatures, the activation energy E_a = 32.2497 kJ/mol and pre-exponential factor A = 47.4132 s^{-1} can be obtained from the linear equation. The relationship between ln k and $1/T$ is shown in Figure 9.

$$k = A\, e^{-E_a/RT} \quad (7)$$

$$\ln k = \ln A - \frac{E_a}{RT} \quad (8)$$

2.3. Macrokinetics. On the basis of previous studies, some hydrodynamic parameters in the falling film tower such as the falling film thickness, Reynolds number, and diffusion coefficient were studied. The falling film thickness can be studied by Nusselt condensation theory.[31] Nusselt was the first one to consider the hydrodynamics associated with laminar falling films and presented eq 9 for falling film thickness

$$\delta_L = \left(\frac{3\mu V_L}{\pi\rho dg}\right)^{1/3} \quad (9)$$

where ρ is the liquid density, d is the inner diameter of the falling film tower, μ is the liquid viscosity, V_L is the liquid volume flow, and v is the liquid flow rate.

The Re number in the falling film tower is shown as eq 10

https://dx.doi.org/10.1021/acsomega.1c00125
ACS Omega 2021, 6, 8394−8402

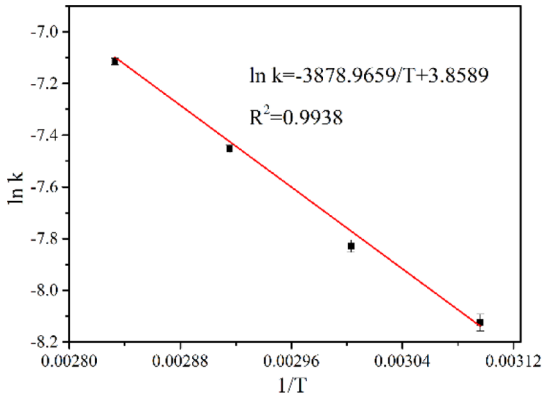

Figure 9. Relationship between ln k and $1/T$.

$$Re = \frac{\rho v d}{\mu} = \frac{4V_L\rho}{\mu\pi d} \tag{10}$$

It was found that the Reynolds numbers at different temperatures are between 261 and 408, which are all less than 2000. The results show that all the falling film flows under experimental conditions behaved as laminar flow. The viscosity of the liquid was measured by a DV3T rheometer, and the density of the reaction solution was measured by a liquid density meter. The results are shown in Figure 10.

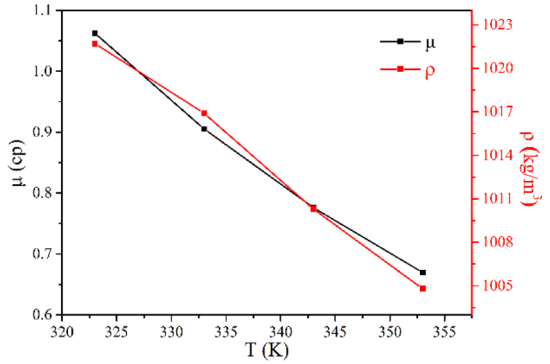

Figure 10. Density and viscosity of the reaction solution at different temperatures.

Figure 11 illustrates the change in liquid film thickness and Reynolds number with temperature; the film thickness δ is between 0.238 and 0.276 mm, which changed regularly within a reasonable range. Because the viscosity of the liquid decreases with increasing temperature, the Reynolds number gradually increases as the temperature rises, while the thickness of the liquid film decreases slightly as the temperature rises.

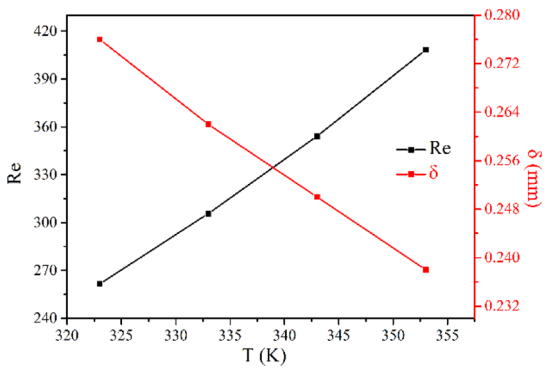

Figure 11. Reynolds number and liquid film thickness at different temperatures.

Since the gas phase of the reaction system is pure oxygen, there is no gas phase resistance in the diffusion of pure gas components, and oxygen is a poorly soluble gas, so the liquid film resistance is much larger than the gas film resistance. Therefore, the gas film resistance can be ignored. For the first-order irreversible reaction, the intrinsic reaction rate eq 11 and mass transfer reaction eq 12 are as follows

$$r = kc_A \tag{11}$$

$$D_A\left(\frac{\partial^2 c_A}{\partial z^2}\right) = \frac{\partial c_A}{\partial t} + kc_A \tag{12}$$

Equations 11 and 12 are analyzed by the double-film model. After introducing steady-state conditions and boundary conditions of liquid film, the macroscopic rate of gas−liquid reaction under the double-film model is as eq 13

$$R_A = k_l\left(c_{Ai} - \frac{c_{Al}}{chHa}\right)\frac{Ha}{thHa} \tag{13}$$

Ha is the Hatta number, which is the basis for judging the relative speed of the intrinsic reaction rate and mass transfer rate. It is defined as the ratio of the possible maximum reaction rate in the film to the possible maximum mass transfer rate in the film. It is an important parameter in the macrokinetics of the gas−liquid reaction. For the first-order irreversible reaction, the Hatta number can be expressed as eq 14

$$Ha = \frac{\sqrt{kD_L}}{k_L} \tag{14}$$

where k_L is the liquid phase mass transfer coefficient and D_L is the liquid phase diffusion coefficient.

According to the double-film theory, the liquid phase mass transfer coefficient k_L can be obtained using eq 15

$$k_L = \frac{D_L}{\delta_L} \tag{15}$$

The liquid phase diffusion coefficient D_L is calculated according to Wilke−Chang (1955) empirical estimation using eq 16:

$$D_{AB} = \frac{7.4 \times 10^{-8}(\phi M_B)^{1/2}T}{\mu_B V_A^{0.6}} \tag{16}$$

where M_B is the molar mass of solvent, μ_B is the viscosity of the solvent, V_A is the molar volume of the solute oxygen at its standard boiling point temperature, and ϕ is the dimensionless association factor of water.

The Reynolds number in the experiment is less than 2000, which indicates that the flow state of the liquid phase is laminar flow. The liquid film can remain relatively static, which conforms to the conditions of the double-film theory and the above equations. The macrokinetic data at different temperatures are shown in Table 3.

The Hatta number obtained in this reaction system fluctuates slightly between 0.072 and 0.080, which is less than 0.3. It can be proved that under this reaction condition, the gas−liquid reaction is a slow reaction, and the mass transfer

https://dx.doi.org/10.1021/acsomega.1c00125
ACS Omega 2021, 6, 8394−8402

Table 3. Macrokinetic Data at Different Temperatures

kinetic parameters	323 K	333 K	343 K	353 K
D_L (m^2/s)	4.264×10^{-9}	5.126×10^{-9}	6.097×10^{-9}	7.153×10^{-9}
k_L (m/s)	1.545×10^{-5}	1.956×10^{-5}	2.439×10^{-5}	3.006×10^{-5}
Ha	0.072	0.073	0.077	0.080

rate is faster than the reaction rate. The reaction is mainly carried out in the main body of the liquid phase, and the oxidation process of Fe(II) to Fe(III) is the rate-limiting step. It also proves that the falling film tower has excellent gas−liquid mass transfer performance and accelerates the gas−liquid mass transfer efficiency in a multiphase reaction. Through the study of kinetics, especially the study of macrokinetics, we have a further understanding of improving the reaction efficiency of α-FeOOH. For example, enlarging the diameter of the falling film tower and tilting the wall of tower appropriately can reduce the *Ha* number, indicating that these adjustments are beneficial to enhance the mass transfer process of the falling film tower. It is also possible to make the tower wall similar to the corrugation of the inner wall of the spherical condenser, which can be tried in future experiments. Alternatively, we can increase the gas−liquid contact area by adding parallel tubes in the falling film tower, which will greatly improve the reaction efficiency.

3. CONCLUSIONS

In conclusion, the process for synthesizing α-FeOOH in a falling film tower with pickling wastewater as a raw material was established. The α-FeOOH crystals synthesized from purified pickling wastewater have good purity and morphology, the purity of α-FeOOH can reach 96.3%, and the iron recovery rate is greater than 90%. Moreover, the intrinsic and macrokinetics were systematically investigated for the first time. For the total reaction rate, the rate-limiting step is the mass transfer process, and for the intrinsic reaction kinetics, the rate-limiting step is the oxidation of Fe(II) to Fe(III). The reaction rate constant k at different temperatures was determined with the activation energy E_a = 32.2497 kJ/mol and the pre-exponential $A = 47.4132\ s^{-1}$. Based on the double-film model, the Reynolds number, liquid film thickness δ, liquid mass transfer coefficient k_L, and Hatta number at different temperatures were obtained. As a result, the *Ha* number of the reaction system at different temperatures is always lower than 0.3. It also proved the excellent gas−liquid mass transfer performance in the falling film tower, which greatly eliminates the limitation of the mass transfer process. Therefore, the production efficiency of this method using the falling film tower is 16 times higher than that of the traditional manufacturing process. The synthesis of α-FeOOH in the falling film tower from pickling wastewater is of great significance for improving the production efficiency of α-FeOOH and the reclamation of pickling wastewater.

4. EXPERIMENTAL SECTION

4.1. Materials. Ferrous sulfate heptahydrate (AR grade), sodium hydroxide (AR grade), and polyacrylamide (AR grade) were provided by Sinopharm Chemical Reagent Co., Ltd. Acid pickling wastewater (industrial waste) was provided by a steel enterprise in Zhejiang, and pure oxygen (>99.5%) was provided by Wuhan Siyu Gas Co., Ltd.

4.2. Characterization. The X-ray diffraction (XRD) of the samples was performed on a Bruker-D8 ADVANCE X-ray diffractometer with Cu Kα radiation (40 kV and 36 mA), 2θ rotation range 10−80°. TEM measurements were taken on a JEM-1400 Plus electron microscope (JEOL, Japan) with an acceleration voltage of 120 kV. The metal compositions of the pickling wastewater and the purified solution were determined by inductively coupled plasma-optical emission spectroscopy (Prodigy 7, Lehman-Leibers, USA) in the wavelength range 165−1100 nm continuous wavelength coverage. The AAS was taken on a CONTRAA-700 (Jena Analytical Instruments AG, Germany) in the wavelength range 185−900 nm. The viscosity of the liquid was measured by a DV3T rheometer (Brookfield Company, USA).

4.3. Synthesis Process. The acid pickling wastewater requires neutralization, filtration, sedimentation, and other purification processes to obtain the purified ferrous solution. First, 10 g of iron scraps was added to 500 mL of pickling wastewater to neutralize the residual acid. At the same time, the Fe^{3+} in the solution was reduced to Fe^{2+}. The reaction solution was heated and boiled until no gas was generated and then filtered to a clear solution. NaOH solution was added to the solution to adjust the pH to around 5.6, and most of the impurity metal ions such as Al^{3+}, Cu^{2+}, Cr^{3+}, and so forth settled in the form of precipitation. Then, a small amount of polyacrylamide was added as the flocculant to adsorb other impurities, and the purified ferrous solution was obtained by filtration. The concentration of ferrous ion in the purified solution is 119.06 g/L. The contents of impurity ions in the solution before and after purified are detailed in the Supporting Information (Tables S1 and S2).

Then, 0.5 mol/L ferrous solution was mixed with the seed crystal solution in a volume ratio of 3:1 (see Supporting Information for seed crystal preparation) and then added to the reaction vessel. After the reaction system was sealed, it was evacuated and replaced with pure oxygen 3 times to make the system a pure oxygen atmosphere. Then, the reaction solution circulated in the falling film tower and made contact with oxygen to react. During the reaction, a PHS-3C pH meter (Shanghai Yidian Scientific Instrument Co., Ltd.) was used to detect the pH of the reaction solution, and the pH of the solution was controlled between 4 and 5 by adding NaOH solution dropwise. After the reaction was complete, the suspension was filtered to obtain a yellow solid powder, the α-FeOOH products were obtained after drying at 80 °C for 3 h. The initial pressure of oxygen in the reaction system was 101.67 kPa, and the pressure at the end of the reaction was only decreased by 1.58 kPa, which accounted for less than 2% of the total pressure. The change in oxygen pressure is negligible and can be regarded as standard atmospheric pressure. Since the consumption of oxygen is extremely low, a sealed pure oxygen atmosphere was used to replace oxygen countercurrent contact when designing the reaction system, thereby greatly reducing the cost.

https://dx.doi.org/10.1021/acsomega.1c00125
ACS Omega 2021, 6, 8394−8402

■ ASSOCIATED CONTENT

Supporting Information

The Supporting Information is available free of charge at https://pubs.acs.org/doi/10.1021/acsomega.1c00125.

Contents of impurity ions in the solution before and after purification, ICP-OES analysis results of pickling wastewater and purified pickling wastewater, and the seed preparation method (PDF)

■ AUTHOR INFORMATION

Corresponding Authors

Yuanyuan Che − *School of Chemistry, Chemical Engineering and Life Sciences, Wuhan University of Technology, Wuhan 430070, Hubei, China*; orcid.org/0000-0003-2883-0762; Email: yyche@whut.edu.cn

Zhipeng Mao − *School of Chemistry, Chemical Engineering and Life Sciences, Wuhan University of Technology, Wuhan 430070, Hubei, China*; Email: ilpclvm@163.com

Authors

Jian Chen − *School of Chemistry, Chemical Engineering and Life Sciences, Wuhan University of Technology, Wuhan 430070, Hubei, China*

Fuwei Xiang − *School of Chemistry, Chemical Engineering and Life Sciences, Wuhan University of Technology, Wuhan 430070, Hubei, China*

Mengjing Zhu − *School of Chemistry, Chemical Engineering and Life Sciences, Wuhan University of Technology, Wuhan 430070, Hubei, China*

Junfeng Li − *School of Chemistry, Chemical Engineering and Life Sciences, Wuhan University of Technology, Wuhan 430070, Hubei, China*

Hongjun Yang − *School of Chemistry, Chemical Engineering and Life Sciences, Wuhan University of Technology, Wuhan 430070, Hubei, China*

Complete contact information is available at: https://pubs.acs.org/10.1021/acsomega.1c00125

Notes

The authors declare no competing financial interest.

■ ACKNOWLEDGMENTS

This research is financially supported by the National Natural Science Foundation of China (21808177) and Fundamental Research Funds of the Central Universities (2019IVB048).

■ NOMENCLATURE

A	pre-exponential (s^{-1})
c	concentration (mol/L)
d	tower diameter (m)
D_L	liquid diffusion coefficient (m^2/s)
E_a	activation energy (kJ/mol)
g	acceleration of gravity (9.81 m/s^2)
Ha	Hatta number
k	reaction rate constant (s^{-1})
k_L	liquid mass transfer coefficient (m/s)
R	molar gas constant (8.314 $J·mol^{-1}·K^{-1}$)
Re	Reynolds number
t	time (min^{-1} or s^{-1})
T	temperature (K)
V_L	liquid volume flow (m^3/s)
ρ	density (kg/m^3)
δ	liquid film thickness (mm)
μ	liquid viscosity (Pa·s or cPa)

■ REFERENCES

(1) Kamada, K.; Hyodo, T.; Shimizu, Y. Visible-Light-Enhanced Electroless Deposition of Nanostructured Iron Oxyhydroxide Thin Films. *J. Phys. Chem. C* **2010**, *114*, 3707−3711.

(2) Choi, J.-W.; Mahendran, B.; Chung, S.-G.; Kim, S.-B.; Lee, S.-H. Surface Modified Mesostructured Iron Oxyhydroxide: Synthesis, Ecotoxicity, and Application. *Water Environ. Res.* **2014**, *86*, 2338−2346.

(3) Huang, S.-C.; Lin, C.-Y. Electrosynthesis, Activation, and Applications of Nickel-Iron Oxyhydroxide in (Photo-)Electrochemical Water Splitting at near Neutral Condition. *Electrochim. Acta* **2019**, *321*, 134667.

(4) Hawash, H. B. I.; Chmielewska, E.; Netriová, Z.; Majzlan, J.; Pálková, H.; Hudec, P.; Sokolík, R. Innovative Comparable Study for Application of Iron Oxyhydroxide and Manganese Dioxide Modified Clinoptilolite in Removal of Zn(II) from Aqueous Medium. *J. Environ. Chem. Eng.* **2018**, *6*, 6489−6503.

(5) Samanta, A.; Das, S.; Jana, S. Exploring β-FeOOH Nanorods as an Efficient Adsorbent for Arsenic and Organic Dyes. *ChemistrySelect* **2018**, *3*, 2467−2473.

(6) Nematollahzadeh, A.; Dabaleh, A.; Ahadi-Jomairan, N.; Torabi, S. Iron-Oxide Nano-Particles Effect on the Blood Hemodynamics in Atherosclerotic Coronary Arteries. *Chem. Eng. Sci.* **2018**, *177*, 293−300.

(7) Li, S.; Qin, G. W.; Zhang, Y.; Pei, W.; Zuo, L.; Esling, C. Anisotropic Growth of Iron Oxyhydroxide Nanorods and Their Photocatalytic Activity. *Adv. Eng. Mater.* **2010**, *12*, 1082−1085.

(8) Garg, S.; Xing, G.; Waite, T. D. Influence of PH on the Kinetics and Mechanism of Photoreductive Dissolution of Amorphous Iron Oxyhydroxide in the Presence of Natural Organic Matter: Implications to Iron Bioavailability in Surface Waters. *Environ. Sci. Technol.* **2020**, *54*, 6771−6780.

(9) Jelle, A. A.; Hmadeh, M.; O'Brien, P. G.; Perovic, D. D.; Ozin, G. A. Photocatalytic Properties of All Four Polymorphs of Nanostructured Iron Oxyhydroxides. *ChemNanoMat* **2016**, *2*, 1047−1054.

(10) Adhikari, M.; Echeverria, E.; Risica, G.; McIlroy, D. N.; Nippe, M.; Vasquez, Y. Synthesis of Magnetite Nanorods from the Reduction of Iron Oxy-Hydroxide with Hydrazine. *ACS Omega* **2020**, *5*, 22440−22448.

(11) Amani-Ghadim, A. R.; Alizadeh, S.; Khodam, F.; Rezvani, Z. Synthesis of Rod-like α-FeOOH Nanoparticles and Its Photocatalytic Activity in Degradation of an Azo Dye: Empirical Kinetic Model Development. *J. Mol. Catal. A: Chem.* **2015**, *408*, 60−68.

(12) Zhang, X.; Wang, X.; Wang, Y.; Li, C.; Feng, H.; Xu, T. Production of Yellow Iron Oxide Pigments by Integration of the Air Oxidation Process with Bipolar Membrane Electrodialysis. *Ind. Eng. Chem. Res.* **2014**, *53*, 1580−1587.

(13) Inohara, D.; Maruyama, H.; Kakihara, Y.; Kurokawa, H.; Nakayama, M. Cobalt-Doped Goethite-Type Iron Oxyhydroxide (α-FeOOH) for Highly Efficient Oxygen Evolution Catalysis. *ACS Omega* **2018**, *3*, 7840−7845.

(14) Patil, D.; Kumar, R.; Xiao, F. Wetting Enhancement of Polypropylene Plate for Falling Film Tower Application. *Chem. Eng. Process.* **2016**, *108*, 1−9.

(15) Li, Y.; Wei, R.; Zhang, R.; Shen, W.; Jin, S. In Silico Modeling of a Novel Refrigeration Process of the Ammonia-Water Falling-Film Absorption. *Ind. Eng. Chem. Res.* **2020**, *59*, 1362−1373.

(16) Abramović, B. F.; Banić, N. D.; Krstić, J. B. Degradation of Thiacloprid by ZnO in a Laminar Falling Film Slurry Photocatalytic Reactor. *Ind. Eng. Chem. Res.* **2013**, *52*, 5040−5047.

(17) Wang, L.; An, S.; Li, Q.; Yu, S.; Wu, S. Phase Change Behavior and Kinetics of CO2 Absorption into DMBA/DEEA Solution in a Wetted-Wall Column. *Chem. Eng. J.* **2017**, *314*, 681−687.

(18) Yu, L.-M.; Zeng, A.-W.; Yu, K. T. Effect of Interfacial Velocity Fluctuations on the Enhancement of the Mass-Transfer Process in Falling-Film Flow. *Ind. Eng. Chem. Res.* **2006**, *45*, 1201−1210.

(19) Domingo, C.; Rodríguez-Clemente, R.; Blesa, M. A. Kinetics of Oxidative Precipitation of Iron Oxide Particles. *Colloids Surf., A* **1993**, *79*, 177−189.
(20) Legg, B. A.; Zhu, M.; Zhang, H.; Waychunas, G.; Gilbert, B.; Banfield, J. F. A Model for Nucleation When Nuclei Are Nonstoichiometric: Understanding the Precipitation of Iron Oxyhydroxide Nanoparticles. *Cryst. Growth Des.* **2016**, *16*, 5726−5737.
(21) Shaddad, M. N.; Cardenas-Morcoso, D.; García-Tecedor, M.; Fabregat-Santiago, F.; Bisquert, J.; Al-Mayouf, A. M.; Gimenez, S. TiO2 Nanotubes for Solar Water Splitting: Vacuum Annealing and Zr Doping Enhance Water Oxidation Kinetics. *ACS Omega* **2019**, *4*, 16095−16102.
(22) Watzky, M. A.; Finke, R. G. Gold Nanoparticle Formation Kinetics and Mechanism: A Critical Analysis of the "Redox Crystallization" Mechanism. *ACS Omega* **2018**, *3*, 1555−1563.
(23) Huang, Z.; Tian, Y.; Gao, Y.; Shao, Z.; Zhang, Y.; Liu, X. Study on the Oxidation Kinetics and Microreactivity of Water-Immersed Coal. *ACS Omega* **2020**, *5*, 17287−17303.
(24) Zhao, H.; Yu, R.; Qiao, H.; Liu, C. Study on the Formation of Glycine by Hydantoin and Its Kinetics. *ACS Omega* **2020**, *5*, 13463−13472.
(25) Ramírez, J. E.; Esquivel-González, S.; Rangel-Mendez, J. R.; Arriaga, S. L.; Gallegos-García, M.; Buitrón, G.; Cervantes, F. J. Biorecovery of Metals from a Stainless Steel Industrial Effluent through Denitrification Performed in a Novel Anaerobic Swirling Fluidized Membrane Bioreactor (ASFMBR). *Ind. Eng. Chem. Res.* **2020**, *59*, 2725−2735.
(26) Zhu, M.; Legg, B.; Zhang, H.; Gilbert, B.; Ren, Y.; Banfield, J. F.; Waychunas, G. A. Early Stage Formation of Iron Oxyhydroxides during Neutralization of Simulated Acid Mine Drainage Solutions. *Environ. Sci. Technol.* **2012**, *46*, 8140−8147.
(27) Lian, J.; Ouyang, Q.; Tsang, P. E.; Fang, Z. Fenton-like Catalytic Degradation of Tetracycline by Magnetic Palygorskite Nanoparticles Prepared from Steel Pickling Waste Liquor. *Appl. Clay Sci.* **2019**, *182*, 105273.
(28) Shrivastava, S.; Rao, S. N. Pickling Waste as an Inexpensive Iron Source for Fenton Oxidation of Synthetic Dye Bath Waste. *Clean: Soil, Air, Water* **2011**, *39*, 996−1000.
(29) Tomaszewska, M.; Gryta, M.; Morawski, A. W. Recovery of Hydrochloric Acid from Metal Pickling Solutions by Membrane Distillation. *Sep. Purif. Technol.* **2001**, *22*−*23*, 591−600.
(30) Zhang, W.; Lu, B.; Tang, H.; Zhao, J.; Cai, Q. Reclamation of Acid Pickling Waste: A Facile Route for Preparation of Single-Phase Fe3O4 Nanoparticle. *J. Magn. Magn. Mater.* **2015**, *381*, 401−404.
(31) Assar, M.; Abolghasemi, H.; Hamane, M. R.; Hashemi, S. J.; Fatoorehchi, H. A New Approach to Analyze Entrance Region Mass Transfer within a Falling Film. *Heat Mass Transfer* **2014**, *50*, 651−660.

https://dx.doi.org/10.1021/acsomega.1c00125
ACS Omega 2021, 6, 8394−8402